# Prevention of Boundary Image Sticking in an AC Plasma Display Panel Using a Vacuum Sealing Process

Choon-Sang Park, Heung-Sik Tae, *Senior Member, IEEE*, Young-Kuk Kwon, Eun Gi Heo, and Byung-Hak Lee

***Abstract*—Boundary image sticking can be inherently prevented in an ac plasma display panel fabricated using a vacuum sealing process. The results indicate that residual impurities, such as nitrogen or oxygen, are essentially related to the production of boundary image sticking. When checking the production of boundary image sticking in a test panel fabricated using a $N_2$ or an $O_2$ flow during the vacuum sealing process, no boundary image sticking appeared in the case of a $N_2$ flow, whereas boundary image sticking was produced with an $O_2$ flow, although the test panel was fabricated using a vacuum sealing process. Consequently, reducing the residual impurity, particularly oxygen, based on a vacuum sealing process can inherently prevent boundary image sticking.**

***Index Terms*—Atmospheric pressure sealing process, boundary image sticking, focused ion beam (FIB), impurity gas, MgO hardness, MgO sputtering rate, nanoindentor, $O_2$ or $N_2$ flow, scanning electron microscope (SEM), time-of-flight secondary ion mass spectrometry (TOF-SIMS), vacuum sealing process, 42-in ac plasma display panel (ac-PDP) module.**

## I. Introduction

IMAGE retention means temporal image sticking that is easily recoverable through minor treatment, whereas image sticking means permanent sticking that is irrecoverable even after serious treatment [1]–[7]. Image sticking is also known to be induced in the nondischarge cells adjacent to the discharge cells, referred to as boundary image sticking [8], [9]. Thus, since human eyes are very sensitive to the edges of an image, boundary image sticking needs to be removed to realize high-image-quality ac plasma display panels (ac-PDPs). In a previous work by the current authors, boundary image sticking was shown to be essentially related to the transportation of the Mg species sputtered from the MgO surfaces of the discharge cells into the adjacent cells [8]. Furthermore, it has been reported that, even in the case permanent boundary image sticking, an aging discharge including both boundary image sticking cells and nonimage sticking cells can restore boundary image sticking cells into normally working cells [9]. However, the inherent prevention of boundary image sticking has not yet been reported. The main issue involved in preventing boundary image sticking is suppressing either the transportation of the sputtered Mg species into the adjacent cells or the reaction of the sputtered Mg species with the MgO surfaces or phosphor layers in the adjacent cells.

Accordingly, based on the idea that the impurity level in a PDP is closely related to the boundary image sticking phenomenon, this paper examined the effects of the vacuum sealing process on boundary image sticking. The corresponding luminance, IR (828 nm) emission, and $V_t$ closed curve for the cells in the nondischarge region adjacent to the discharge region $(=$ boundary image sticking cells$)$ were observed in comparison with the nondischarge region far away from the discharge region $(=$ normally working cells$)$ under two different image patterns, i.e., dark and full-white backgrounds, after two different sealing processes. In addition, the effect of an $O_2$ or a $N_2$ flow during the vacuum sealing process on boundary image sticking was also examined to check which impurity factor was dominant, $O_2$ or $N_2$.

## II. Experimental Setup

Fig. 1(a) and (b) shows a schematic of the conventional atmospheric pressure sealing and proposed vacuum sealing processes used for the 42-in test panels, respectively [10]. In both cases, the MgO surfaces in the 42-in test panels were grown using exactly the same growth method (i.e., the ion-plating method, not shown here), and only the sealing processes were different. As shown in Fig. 1(a), with the conventional sealing process, the front and rear glass was initially sealed under an atmospheric pressure of 760 torr. A high vacuum pump was then used to evacuate the panel through a glass tip located in the corner of the rear glass. In this case, the base vacuum level of the test panel was limited by the pumping conductance, which was mainly determined by the barrier rib shape. For the test panel with a box-type barrier rib, the base vacuum level achieved in the center region and a region located far away from the glass tip was $10^{-2}$ torr, although the base vacuum level achieved in the region located near the glass tip was $10^{-5}$ torr, as shown in Fig. 1(a). After tipping off the test panel at a pressure of $10^{-2}$ torr, the gas was filled to a pressure of 430 torr. Meanwhile, to achieve a high base vacuum level with a low pressure, a vacuum sealing process was adopted.

Manuscript received August 8, 2007; revised March 11, 2008. This work was supported in part by the New Growth Engine project of the Ministry of Commerce, Industry and Energy of Korea and in part by the Brain Korea 21 (BK21). The review of this paper was arranged by Editor D. Verret.

C.-S. Park and H.-S. Tae are with the School of Electrical Engineering and Computer Science, Kyungpook National University, Daegu 702-701, Korea (e-mail: hstae@ee.knu.ac.kr).

Y.-K. Kwon, E. G. Heo, and B.-H. Lee are with the Plasma Display Panel Division, Samsung SDI Company, Ltd., Cheonan City 330-300, Korea.

Color versions of one or more of the figures in this paper are available online at http://ieeexplore.ieee.org.

Digital Object Identifier 10.1109/TED.2008.921986

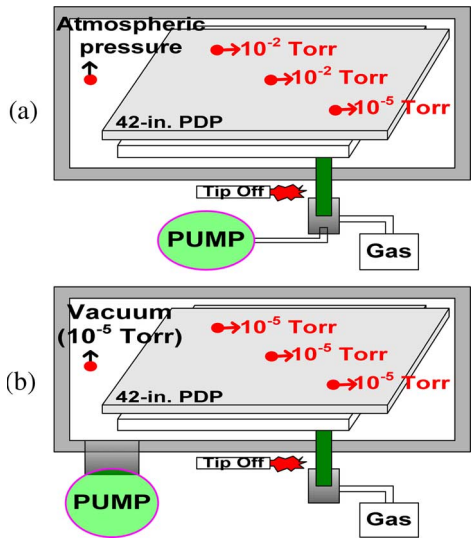


Fig. 1. Schematic of (a) conventional atmospheric pressure sealing and (b) proposed vacuum sealing processes.

As shown in Fig. 1(b), the vacuum sealing process involved sealing the front and rear glass in a high vacuum chamber, then evacuating the sealing chamber, instead of using a glass tip and a high vacuum pump, resulting in a base vacuum level of about $10^{-5}$ torr [10]. Thereafter, similar to Fig. 1(a), the panel was tipped off at a pressure of $10^{-5}$ torr, and the gas was filled to a pressure of 430 torr. However, vacuum sealing is known to create difficulties as regards the adhesion between the front and rear glass, since conventional glass sealing frits only produce good adhesion under high-pressure conditions, thereby hindering the adoption of a vacuum sealing process in the fabrication of commercial ac-PDPs. Consequently, this experiment employed a new glass sealing frit with a good adhesion under low-pressure conditions during the vacuum sealing process. Fig. 2 shows the optical measurement systems and a 42-in ac-PDP module with three electrodes used in the experiment, where X is the sustain electrode, Y is the scan electrode, and Z is the address electrode. To produce permanent boundary image sticking, the entire region of the 42-in test panel was changed to a dark background (about 0.1 cd/m$^2$) or a full-white background (about 175 cd/m$^2$) immediately after displaying a square-type image (region A) at a peak luminance (about 1000 cd/m$^2$) for about 500 h [8]. The frequency for the sustain period was 200 kHz, and the sustain voltage was 206 V. A driving method with a selective reset waveform was also adopted. The detailed panel specifications for the two cases were exactly the same as those in [8], except for the sealing process.

## III. Boundary Image Sticking Phenomena With Vacuum Sealing and Conventional Sealing Processes

### A. Images and Luminance With Dark and Full-White Backgrounds

Fig. 3(a)–(d) shows the image sticking patterns and luminance differences for regions A, B, and C with a dark background captured from the test panels fabricated by the two different sealing processes, where Fig. 3(a) and (b) shows the conventional sealing case, whereas Fig. 3(c) and (d) shows the vacuum sealing case. In Fig. 3, region A represents the discharge region, region B represents a nondischarge region adjacent to the discharge region A, and region C represents a nondischarge region far away from the discharge region A. For the conventional sealing case, image sticking was clearly observed in regions A and B, as shown in Fig. 3(a). Moreover, a luminance difference was also observed between regions B and C, as shown in Fig. 3(b) [8]. However, for the proposed vacuum sealing case, no image sticking was observed in region B (i.e., boundary image sticking region), and no luminance difference was observed between regions B and C, as shown in Fig. 3(c) and (d), respectively. Fig. 4(a)–(d) shows the image sticking patterns and luminance differences for regions A, B, and C with a full-white background captured from the test panels fabricated using the two different sealing processes, where Fig. 4(a) and (b) shows the conventional sealing case, whereas Fig. 4(c) and (d) shows the proposed vacuum sealing case. For the conventional case, as with a dark background, image sticking was observed in regions A and B with a full-white background, whereas in contrast to the results with a

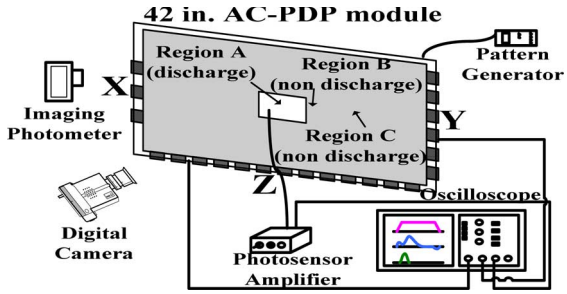


Fig. 2. Schematic of an experimental setup used to monitor the boundary image sticking phenomenon.

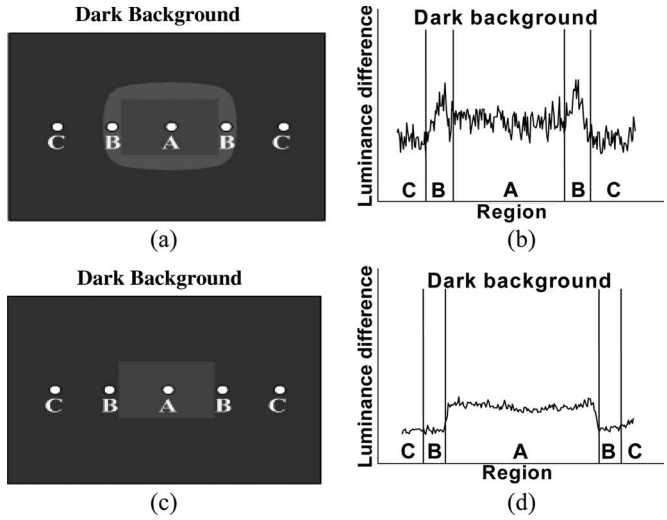


Fig. 3. Image sticking patterns and luminance differences for regions A, B, and C with a dark background captured from test panels fabricated using two different sealing processes. (a) and (b) Conventional sealing case. (c) and (d) Proposed vacuum sealing case.

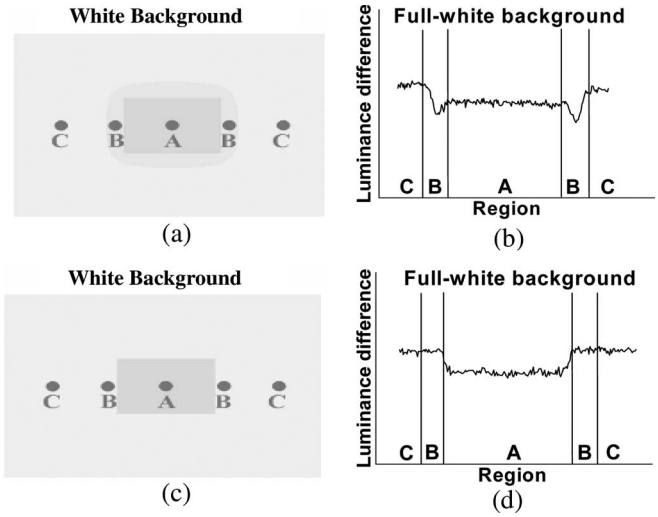


Fig. 4. Image sticking patterns and luminance differences for regions A, B, and C with a full-white background captured from test panels fabricated using two different sealing processes. (a) and (b) Conventional sealing case. (c) and (d) Proposed vacuum sealing case.

dark background, the luminance in region B was observed to be lower than that in region C or A, as shown in Fig. 4(a) and (b), respectively [8]. Meanwhile, for the proposed vacuum sealing case, as with a dark background, no image sticking was observed in region B (i.e., boundary image sticking region) with a full-white background, and no luminance difference was observed between regions B and C, as shown in Fig. 4(c) and (d), respectively.

### *B. IR Emissions During the Reset Period With a Dark Background and During the Sustain Period With a Full-White Background*

Fig. 5(a) and (b) shows a comparison of the IR (828 nm) emissions measured for regions A, B, and C during the reset period with a dark background. For temporal image sticking, the discharge region has the lowest firing voltage, causing a brighter background luminance [2], [5], [6]. Conversely, for permanent image sticking, the discharge region has the highest firing voltage, causing a lower background luminance [8]. In the conventional sealing case, the IR peak for region B was shifted to the left compared to that for regions A and C [8], as shown in Fig. 5(a), whereas in the vacuum sealing case, the ignition time and intensity of the IR (828 nm) emission waveforms were no different between regions B and C, as shown in Fig. 5(b). Furthermore, in the vacuum sealing case, the IR peak during the ramp-up period was shifted to the left and intensified compared to that in the conventional sealing case, indicating that the reset discharge was efficiently initiated at a lower voltage in the former case, resulting in the accumulation of lots of wall charges during the ramp-up period. Thus, the higher IR peak monitored during the ramp-down period was due to the many wall charges accumulated during the ramp-up period [10]. Meanwhile, Fig. 6(a) and (b) shows a comparison of the IR (828 nm) emissions measured for regions A, B, and C during the sustain period with a full-white background. In the conventional sealing case, the IR emission data in Fig. 6(a) revealed that the

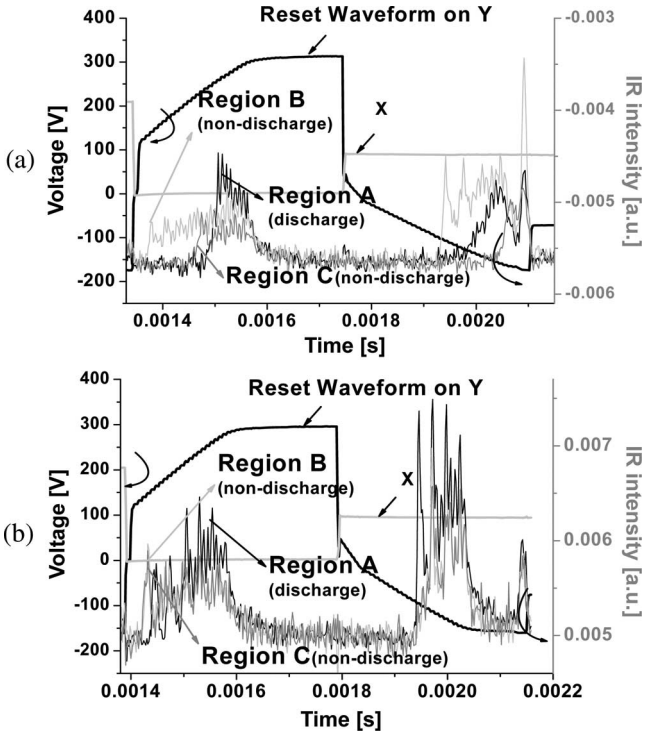


Fig. 5. Comparison of IR (828 nm) emissions measured for regions A, B, and C during reset period with a dark background in test panels fabricated using two different sealing processes. (a) Conventional sealing case. (b) Proposed vacuum sealing case.

IR peaks for region B were intensified compared to those for region C, whereas in the vacuum sealing case, the ignition time and intensity of the IR emission waveforms were no different between regions B and C, as shown in Fig. 6(b).

### *C. Firing Voltages Using $V_t$ Closed Curves*

Fig. 7(a) and (b) shows a comparison of the $V_t$ closed curves measured for regions A, B, and C. In the conventional sealing case, for region B, the firing voltages for the surface and plate-gap discharges under MgO cathode conditions and the plate-gap discharges under phosphor cathode conditions were slightly decreased by about 10–12 and 8–16 V, respectively, in comparison with those for region C, as shown in Fig. 7(a). In this case, the reduction in the firing voltage for the surface and plate-gap discharges was presumably due to Mg deposition on the MgO and phosphor layers, caused by the Mg species sputtered from region A [8], [9]. In the vacuum sealing case, to investigate the main factor for the absence of any difference in the luminance and IR characteristics between regions B and C, the $V_t$ closed curve was measured in three regions, namely A, B, and C, respectively, as shown in Fig. 7(b). The firing voltages under phosphor and MgO cathode conditions in regions B and C were almost the same in the vacuum sealing case, implying that the Mg species sputtered from the discharge cells (region A) did not induce a reaction with the MgO surface and phosphor layer in the boundary image sticking cells (region B). Consequently, the $V_t$ closed curve analysis confirmed that the vacuum sealing process contributed to the inherent prevention of boundary image sticking.

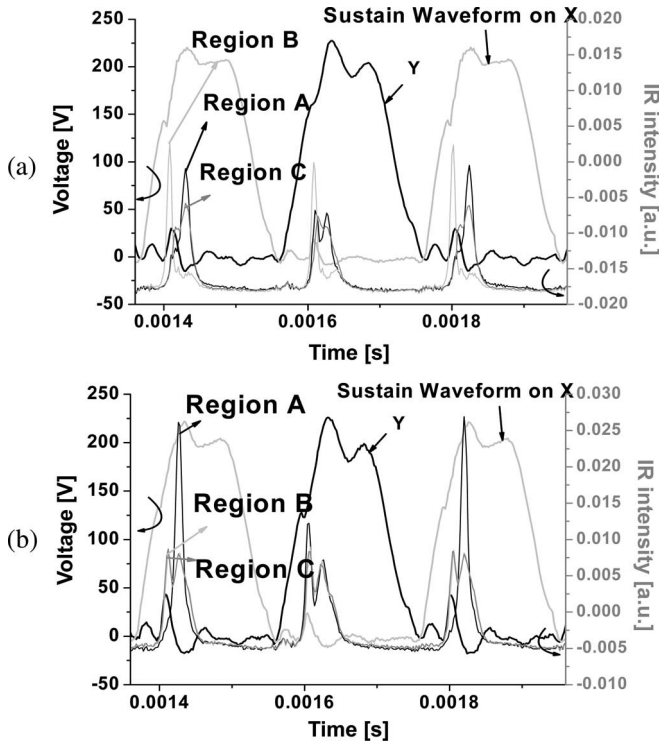


Fig. 6. Comparison of IR (828 nm) emissions measured from regions A, B, and C during the sustain period with a full-white background in test panels fabricated using two different sealing processes. (a) Conventional sealing case. (b) Proposed vacuum sealing case.

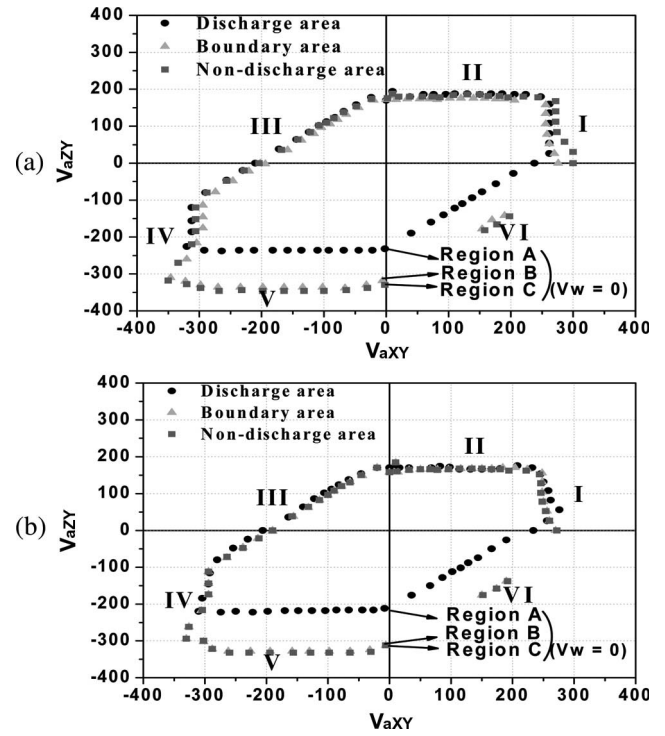


Fig. 7. Comparison of $V_t$ closed curves measured for regions A, B, and C in test panels fabricated using two different sealing processes. (a) Conventional sealing case. (b) Proposed vacuum sealing case.

A scanning electron microscope (SEM) and time-of-flight secondary ion mass spectrometry (TOF-SIMS) were also used to inspect the MgO surface change and deposition of sputtered

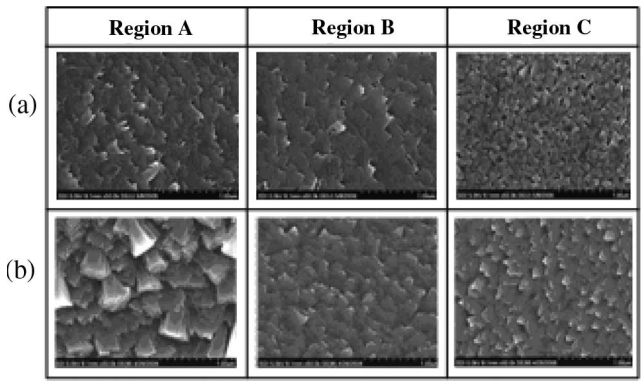


Fig. 8. Comparison of SEM images of MgO surface changes in regions A, B, and C after a 500-h sustain discharge in test panels fabricated using two different sealing processes. (a) Conventional sealing case. (b) Proposed vacuum sealing case.

Mg on the phosphor layer in the boundary image sticking cells for the two different sealing cases. Fig. 8(a) and (b) shows a comparison of the SEM images of the MgO surface changes in regions A, B, and C after the 500-h sustain discharge. In both cases, the MgO surfaces in region A were sputtered or damaged due to severe ion bombardment during the 500-h strong sustain discharge; thus, the resultant surfaces were rough, and the grain sizes were relatively larger, in comparison with the MgO surface in region C, i.e., the nondischarge region far away from the discharge region. However, the changes in the MgO surface in region B, i.e., the boundary image sticking region, were quite different for the two cases. In the conventional sealing case, the morphology of the MgO surface in region B was similar to that in region A with a relatively large grain size. Thus, the surface change in region B, where no discharge was produced, was presumably due to the redeposition of the Mg transported from region A, where the MgO surface was sputtered during the iterant strong sustain discharge [8]. Conversely, in the vacuum sealing case, the morphology of the MgO surface in region B was almost similar to that in region C, as shown in Fig. 8(b). Unlike the conventional sealing case, the grain size of the MgO surface in region B was relatively small, such as that in region C. Consequently, no redeposition of the Mg transported from region A appeared to occur in the vacuum sealing case.

Fig. 9(a) and (b) shows a comparison of the Mg profiles for the red phosphor layers in regions A, B, and C based on a TOF-SIMS analysis. In the conventional sealing case, the Mg intensity in regions A and B shifted upward compared to that in region C, as shown in Fig. 9(a), indicating that the Mg was redeposited on the phosphor layer. Although the sputtered Mg was predominantly redeposited in region A, there was also a slight redeposition in region B. However, in the vacuum sealing case, the Mg intensity detected in region B was almost similar to that for the cells in region C, as shown in Fig. 9(b). Since the redeposition of the Mg on the phosphor layer significantly affects the discharge characteristics, particularly under phosphor cathode conditions, the same Mg intensities detected in regions B and C, as shown in Fig. 9(b), indicated that the discharge and related luminance characteristics in regions B and C were also very similar.

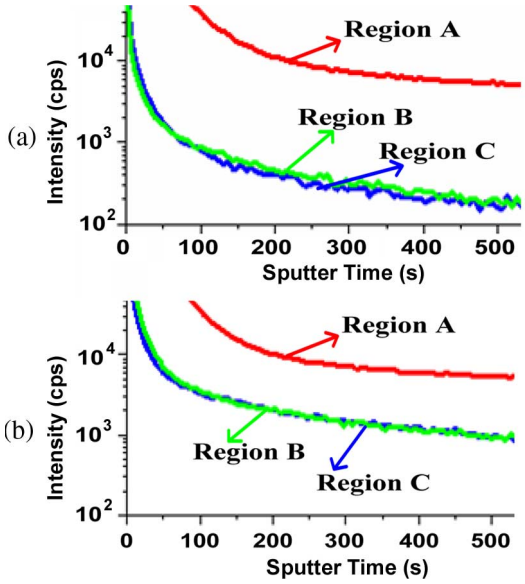


Fig. 9. Comparison of Mg profiles for red phosphor layers in regions A, B, and C using a TOF-SIMS analysis in test panels fabricated using two different sealing processes. (a) Conventional sealing case. (b) Proposed vacuum sealing case.

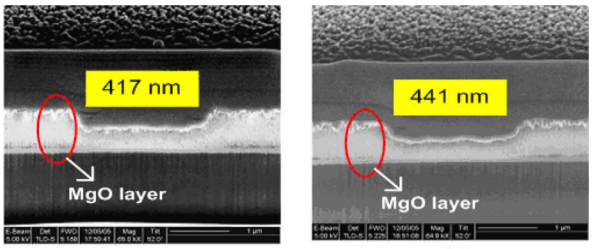


Fig. 10. Comparison of MgO sputtering rates using an FIB in test panels fabricated using two different sealing processes. (a) Conventional sealing case. (b) Proposed vacuum sealing case.

### *D. Sputtering Rates and Hardness of MgO Layers*

Fig. 10(a) and (b) shows a comparison of SEM cross-sectional images of the sputtered MgO layers when using a focused ion beam (FIB). In Fig. 10, the FIB was used to measure the rate of the MgO sputtered from the MgO layer when Ga ions (30 keV) struck the MgO surface for 105 s. As shown in Fig. 10(a) and (b), the sputtering rate of the MgO layer in the vacuum sealing case was higher than that in the conventional sealing case. Meanwhile, Fig. 11 shows a comparison of the hardness of the MgO layer when using a nanoindentor. In Fig. 11, the nanoindentation means the dug depth and area of the MgO layer when depressing a nanosized Berkovich indentation particle onto the surface of the MgO layer. As shown in Fig. 11, the MgO layer in the vacuum sealing case was softer compared to that in the conventional sealing case. As such, this increase in the MgO sputtering rate resulting from a decrease in the MgO surface hardness in the case of the vacuum sealing may have been caused by an increase in the oxygen vacancy of the MgO layer due to the high-vacuum-sealed conditions. Therefore, the results in Figs. 10 and 11

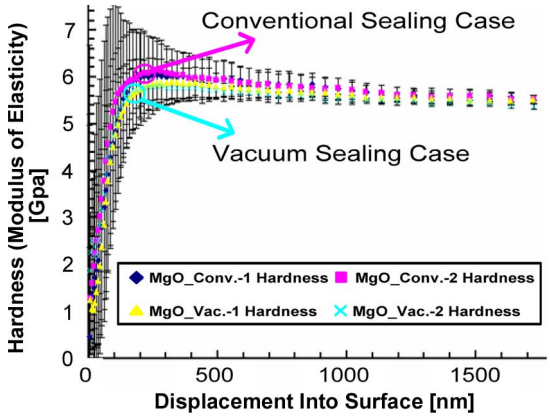


Fig. 11. Comparison of MgO hardness of MgO layers using a nanoindentor in test panels fabricated using two different sealing processes: conventional sealing and proposed vacuum sealing.

indicate that the MgO surface characteristics could be changed by simply controlling the sealing pressure without modifying the MgO growth conditions. The change in the sealing pressure from $10^{-2}$ to $10^{-5}$ torr caused a softer MgO surface, thereby increasing the Mg species sputtered during the 500-h strong sustain discharge. However, contrary to the expectation that an increase in the Mg sputtered in the discharge region A would facilitate the transportation of the sputtered Mg species into the nondischarge cells adjacent to the discharge region A, i.e., region B, resulting in more severe boundary image sticking, the experimental results showed that the vacuum sealing completely inhibited boundary image sticking, even after a strong sustain discharge was continuously produced for about 500 h. Consequently, these results mean that the MgO and phosphor surfaces of the cells in the boundary image sticking region did not change, irrespective of the transportation of the Mg species sputtered from the discharge cells. In other words, it would appear that the reduced impurity level, such as $O_2$, contributed to suppressing the reaction (i.e., redeposition) between the MgO and the phosphor surface in the boundary image sticking cells, i.e., nondischarge cells, despite the increased Mg sputter rate of the discharge cells due to the vacuum sealing process. However, in contrast to the boundary image sticking, the permanent image sticking of the discharge cells was more severe with the vacuum sealing process due to the increase in the Mg sputter rate of the discharge cells.

## IV. Analysis of Prohibition of Boundary Image Sticking Induced by a Vacuum Sealing Process

### *A. Monitoring of an $O_2$ or a $N_2$ Gas Flow During a Vacuum Sealing Process Using $V_t$ Closed Curves*

The experimental results for the vacuum sealing process confirmed that the inherent prevention of boundary image sticking was mainly related to the reduction of residual impurities, including oxygen or nitrogen, caused by lowering the sealing pressure. Thus, to check the effect of $O_2$ or $N_2$ as the dominant factor of residual impurity in terms of preventing boundary image sticking, $O_2$ or $N_2$ gas was allowed to flow during the

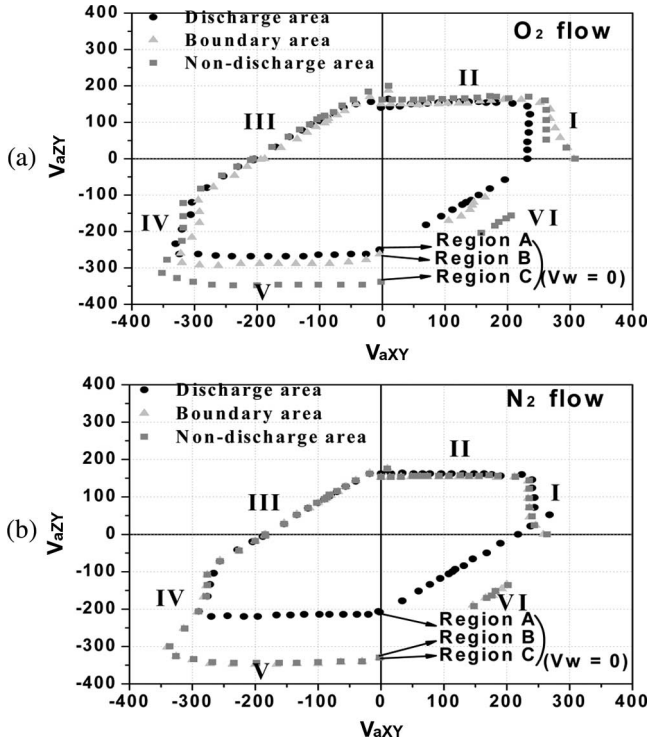


Fig. 12. Comparison of $V_t$ closed curves measured for regions A, B, and C in a test panel fabricated using a vacuum sealing method during (a) $O_2$ and (b) $N_2$ flow.

vacuum sealing process. Despite the vacuum sealing process, the test panel fabricated using an $O_2$ flow during the vacuum sealing process exhibited even more boundary image sticking than the test panel fabricated using the conventional sealing process, which was also confirmed by the $V_t$ closed curve data in Fig. 12(a). In the case of an $O_2$ flow, the firing voltages in region B for the surface and plate-gap discharges under MgO cathode conditions and the plate-gap discharges under phosphor cathode conditions were decreased by about 10–26 and 46–78 V, respectively, in comparison with those in region C, as shown in Fig. 12(a). However, in the case of a $N_2$ flow, no boundary image sticking was observed, which was also confirmed by the $V_t$ closed curve data in Fig. 12(b). Therefore, these results demonstrated that the inherent prevention of boundary image sticking was essentially related to the reduction of the residual impurity, particularly $O_2$, resulting from the vacuum sealing process.

### *B. Monitoring of Boundary Image Sticking in a Test Panel Fabricated by an $O_2$ Gas Flow During a Vacuum Sealing Process*

As shown in Fig. 13(a)–(d), in the case of an $O_2$ flow during the vacuum sealing process, boundary image sticking patterns and luminance differences between regions B and C were observed with both dark and full-white backgrounds after displaying the square-type image (region A) for about 500 h. In addition, as shown in Fig. 14(a) and (b), when using an $O_2$ flow during the vacuum sealing process, the IR peak for region B was shifted to the left when compared to that for regions

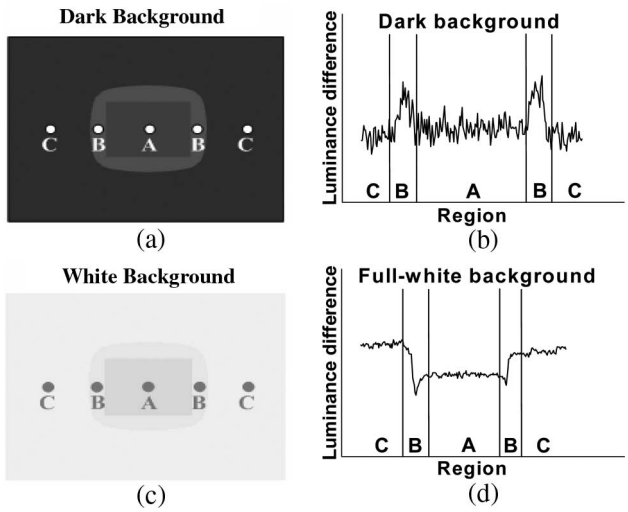


Fig. 13. (a) Image sticking pattern and (b) luminance difference for regions A, B, and C with a dark background, and (c) image sticking pattern and (d) luminance difference for regions A, B, and C with a full-white background after an iterant 500-h strong sustain discharge with a square-type image, as shown in Fig. 2, captured from the test panel fabricated using an $O_2$ gas flow during a vacuum sealing process.

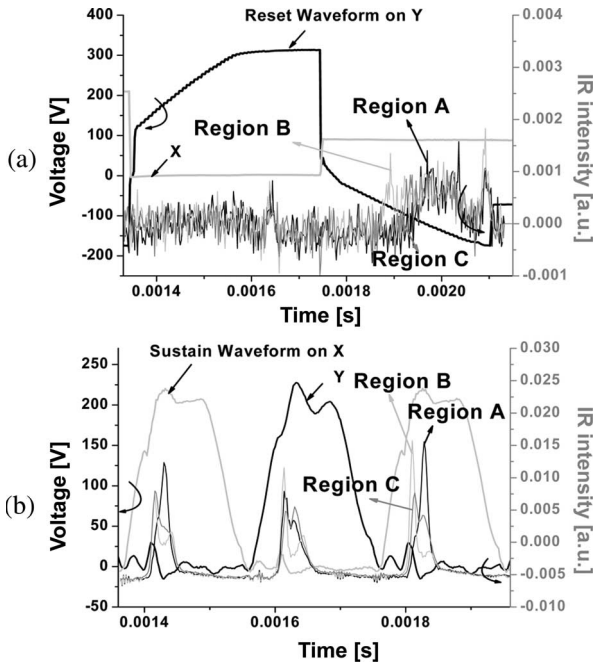


Fig. 14. Comparison of IR (828 nm) emissions measured for regions A, B, and C in a test panel fabricated using an $O_2$ gas flow during a vacuum sealing process during reset and sustain periods with (a) dark and (b) full-white backgrounds.

A and C during the ramp-falling period and also intensified when compared to that for region C during the sustain period. Consequently, as a result of monitoring the boundary image sticking in the test panel fabricated using an $O_2$ gas flow during the vacuum sealing process, the oxygen level was shown to have a significant influence on production of boundary image sticking, confirming that a vacuum sealing process that can reduce the impurity level, particularly $O_2$, can contribute to the inherent prevention of boundary image sticking.

## V. Conclusion

The vacuum sealing process used to enhance the base vacuum level from $10^{-2}$ to $10^{-5}$ torr produced a softer MgO surface and thereby increased the Mg sputter rate in the discharge cells. Nonetheless, no changes were observed in the MgO surface and phosphor layer in the adjacent cells, i.e., the boundary image sticking region, indicating that the reduced impurity level, such as $O_2$, suppressed any reaction between the MgO surface and phosphor layer in the adjacent cells caused by the transportation of the Mg sputtered from the discharge cells. However, despite the vacuum sealing process, the use of an $O_2$ flow induced severe boundary image sticking. Consequently, the results demonstrated that it was the low $O_2$ impurity level of the test panel fabricated using the vacuum sealing process that essentially enabled the inherent prevention of boundary image sticking in the adjacent cells, even when a strong sustain discharge was continuously produced in the discharge cells.

## References


[1] J.-W. Han, H.-S. Tae, B. J. Shin, S.-I. Chien, and D. H. Lee, "Experimental observation of temperature-dependent characteristics for temporal dark boundary image sticking in 42-in. AC-PDP," *IEEE Trans. Plasma Sci.*, vol. 34, no. 2, pp. 324–330, Apr. 2006.

[2] H.-S. Tae, C.-S. Park, B.-G. Cho, J.-W. Han, B. J. Shin, S.-I. Chien, and D. H. Lee, "Driving waveform for reducing temporal dark image sticking in AC plasma display panel based on perceived luminance," *IEEE Trans. Plasma Sci.*, vol. 34, no. 3, pp. 996–1003, Jun. 2006.

[3] L. C. Pitchford, J. Wang, D. Piscitelli, and J.-P. Boeuf, "Ion and neutral energy distributions to the MgO surface and sputtering rates in plasma display panel cells," *IEEE Trans. Plasma Sci.*, vol. 34, no. 2, pp. 351–359, Apr. 2006.

[4] T. Kosaka, K. Sakita, and K. Betsui, "Firing voltage fluctuation phenomenon caused by gas density nonuniformity in PDPs," in *Proc. IDW/AD Dig.*, 2005, pp. 1469–1472.

[5] H.-S. Tae, J.-W. Han, S.-H. Jang, B.-N. Kim, B. J. Shin, B.-G. Cho, and S.-I. Chien, "Experimental observation of image sticking phenomenon in AC plasma display panel," *IEEE Trans. Plasma Sci.*, vol. 32, no. 6, pp. 2189–2196, Dec. 2004.

[6] H.-J. Lee, D.-H. Kim, Y.-R. Kim, M.-S. Hahm, D.-K. Lee, J.-Y. Choi, C.-H. Park, J.-W. Rhyu, J.-K. Kim, and S.-G. Lee, "Analysis of temporal image sticking in AC-PDP and the methods to reduce it," in *Proc. SID Dig.*, 2004, pp. 214–217.

[7] B. J. Shin, K. C. Choi, and J. H. Seo, "Effects of pre-reset conditions on reset discharge from ramp reset waveforms in AC plasma display panel," *IEEE Trans. Electron Devices*, vol. 52, no. 1, pp. 17–22, Jan. 2005.

[8] C.-S. Park, H.-S. Tae, Y.-K. Kwon, and E. G. Heo, "Experimental observation of halo-type boundary image sticking in AC plasma display panel," *IEEE Trans. Electron Devices*, vol. 54, no. 6, pp. 1315–1320, Jun. 2007.

[9] C.-S. Park, H.-S. Tae, Y.-K. Kwon, and E. G. Heo, "Recovery of boundary image sticking using aging discharge in AC plasma display panel," *IEEE Trans. Plasma Sci.*, vol. 35, no. 5, pp. 1315–1320, Oct. 2007.

[10] C.-S. Park, H.-S. Tae, Y.-K. Kwon, S. B. Seo, E. G. Heo, and B.-H. Lee, "Discharge characteristics of 42-in. AC-plasma display panel fabricated by vacuum sealing method," in *Proc. SID Dig.*, 2007, pp. 1617–1620.



**Choon-Sang Park** received the M.S. degree in electronic and electrical engineering from Kyungpook National University, Daegu, Korea, in 2006, where he is currently working toward the Ph.D. degree in electronic engineering.

His current research interests include plasma physics and driving waveform of plasma display panels.



**Heung-Sik Tae** (M'00–SM'05) received the B.S., M.S., and Ph.D. degrees in electrical engineering from Seoul National University, Seoul, Korea, in 1986, 1988, and 1994, respectively.

Since 1995, he has been a Professor with the School of Electrical Engineering and Computer Science, Kyungpook National University, Daegu, Korea. His research interests include the optical characterization and driving waveform of plasma display panels.

Dr. Tae is a member of the Society for Information Display. He has been serving as an Editor of the IEEE Transactions on Electron Devices section on display technology since 2005.



**Young-Kuk Kwon** received the B.S. degree in chemical science from Keimyung University, Daegu, Korea, in 1995 and the M.S. degree in chemical science from Kyungpook National University, Daegu, in 1997.

He is currently a Manager with the Plasma Display Panel Division, Samsung SDI Company, Ltd., Cheonan City, Korea. His current research interests include plasma discharge and panel design of plasma display panels.



**Eun Gi Heo** received the B.S. degree in physical science from Seoul National University, Seoul, Korea, in 1988 and the M.S. and Ph.D. degrees from Korea Advanced Institute of Science and Technology, Taejon, Korea, in 1990 and 1996, respectively.

He is currently a General Manager with the Development Team, Plasma Display Panel Division, Samsung SDI Company, Ltd., Cheonan City, Korea. His current research interests include plasma physics and panel design of plasma display panels.



**Byung-Hak Lee** received the B.S. degree in metallurgical engineering from Sungkyunkwan University, Suwon, Korea, in 1980 and the M.S. and Ph.D. degrees in materials science and engineering from the University of Texas, Austin, in 1989 and 1995, respectively.

He is currently a Vice President with the Development Team, Plasma Display Panel Division, Samsung SDI Company, Ltd., Cheonan City, Korea. His current research interests include plasma physics and panel design of plasma display panels.